American Mineralogist, Volume 89, pages 485–491, 2004

Unoccupied states of pyrite probed by electron energy-loss spectroscopy (EELS)

LAURENCE A.J. GARVIE[1,*] AND PETER R. BUSECK[1,2]

[1]Department of Geological Sciences, Arizona State University, Tempe, Arizona 85287-1404, U.S.A.
[2]Department of Chemistry/Biochemistry, Arizona State University, Tempe, Arizona 85287-1604, U.S.A.

ABSTRACT

Electron energy-loss spectra (EELS) of pyrite (FeS_2) were acquired and include the Fe *K*, $L_{2,3}$, $M_{2,3}$, and M_1 edges, and the S *K*, $L_{2,3}$, and L_1 edges. The core-loss edges exhibit a range of shapes and different theories are required to understand the spectra. In the process a clear picture of the conduction-band states as a function of energy above the band gap is obtained. This analysis reveals the extent of mixing of unoccupied states and thus provides an understanding of the limits of interpreting core-loss edges in light of the optical dipole limit. A unified picture of the unoccupied states is obtained by aligning the spectra on a common energy scale relative to the published Bremsstrahlung isochromat spectrum (BIS) and with the results of band structure calculations. This alignment allows similarities between the spectra of different atoms to be related to mixing of local conduction-band states. The coincidence of the Fe *K* and S $L_{2,3}$ spectral features attests to the strong hybridization of the Fe *p*-S 3*d* states. The main Fe $L_{2,3}$ edges are followed by structures that confirm an Fe-S bond with a substantial degree of mixing between Fe d^6 and d^7 states. The aligned EELS spectra clearly divide the unoccupied states into two regions. The first region is dominated by the intense *d*-like component of the Fe L_3 edge and *p*-like components of the S *K* and L_1 edges. A small pre-peak at the Fe *K* edge aligned with the Fe $L_{2,3}$ edge peak maximum is indicative of Fe $4p + 3d\ e_g$ and S 3*p* mixing. Similarly, the pre-peak to the S $L_{2,3}$ edge arises from transitions to states with mixed S $s + p +$ Fe $3d\ e_g$ character.

INTRODUCTION

Pyrite is the most abundant and widespread natural sulfide at the Earth's surface, occurring in ore deposits and common in many sedimentary, metamorphic, and igneous rocks. It is the main Fe sulfide in porphyry copper deposits and its decomposition in mine dumps is of concern because of the generation of toxic effluent. An understanding of its dissolution and sorption properties can only be fully understood if its bonding properties are fully revealed. Pyrite is a semiconducting 3*d* transition metal (TM) dichalcogenide with a band gap of ca. 0.95 eV and a refractive index of between 3.5 to 5 (Sato 1984; Ferrer et al. 1990; de las Heras and Lifante 1997). Interest has focused on pyrite because of its promising capabilities as a photovoltaic (Ennaoui et al. 1993). In addition, the MS_2 dichalcogenides with the pyrite structure exhibit a range of electronic, magnetic, and optical properties that are of technological interest.

A molecular orbital picture of pyrite describes the bonding in terms of $(S_2)^{2-}$ pairs that lead to five occupied S states per pair; the remaining antibonding S $p\sigma^*$ states are located above the band gap. Iron is in a $3d^6$ state and has a low-spin $3d(t_{2g})^6(e_g)^0$ configuration, as confirmed by Mössbauer and XAS spectroscopy (Thole and van der Laan 1988; Schmidbeurmann and Lottermoser 1993). The Fe 3*d* states are separated by crystal-field splitting into a lower t_{2g} level in the valence band, and an upper e_g level in the conduction band (Eyert et al. 1998; Opahle et al. 1999). The Fe $3d\ e_g$-states form σ bonds and have a large overlap with the S 3*p* orbitals (Raybaud et al. 1997). The S $3p_z$ states dominate over the $3p_x$ and $3p_y$ states in the conduction band (Eyert et al. 1998). The S $3p_z$ states form σ bonds between the two S atoms of a pair whereas the $3p_x$ and $3p_y$ orbitals experience a smaller overlap via π bonds.

A thorough understanding of the unoccupied states usually lags behind that of the occupied states. These unoccupied states can be efficiently explored by the excitation of core electrons by fast electron bombardment (Egerton 1996). Electron energy-loss spectroscopy (EELS) is an efficient method for elemental quantification, and the shapes of the spectra provide important information regarding bonding and local electronic structure. A major advantage of EELS with a transmission electron microscope (TEM) compared to other spectroscopies is its high spatial resolution, which can be as small as 1 Å. Detailed analysis of core-loss edge features is possible through comparison of the edge shapes with the results of ab initio calculations.

An EELS spectrum represents transitions from core electrons to unoccupied states. These spectra can usually be related to the unoccupied density of states. However, this transition process is local and governed by dipole selection rules, so the spectrum displays the site and symmetry-selected density of states (DOS). The site refers to the element that is probed and the symmetry to the orbital character of a scattered electron.

Only non-bonded electrons form core-loss edges. For example, Fe has a ground-state electronic configuration $[Ar]3d^64s^2$. When bonded to S in pyrite it can be considered to be $Fe^{2+}(S_2)^{2-}$ and so has the configuration $[Ar]3d^6$. In addition, the 3*d* electrons are hybridized with the S *p* orbitals and so do not form core-loss edges. Therefore, the Fe core-loss edges that are possible include *K*, L_1, $L_{2,3}$, M_1, and $M_{2,3}$ involving transitions from 1*s*, 2*s*, 2*p*, 3*s*, and 3*p* levels, respectively. The $3d^6$ and $4s^2$ electrons constitute part of the valence band and therefore contribute to the optical

* E-mail: lgarvie@asu.edu

properties of the solid and are visible as interband transitions of the plasmon region of the EELS spectrum.

Individual core-loss edges can provide important information about an atom. Some applications include the identification of metal valence as well as the determination of mixed-valence ratios (Garvie et al. 1994; Garvie and Buseck 1998; Frost et al. 2001; van Aken and Liebscher 2002; Zega et al. 2003), distinction between low- and high-spin states (Collison et al. 1997), determination of coordination and coordination ratios (Hansen et al. 1994; Gloter et al. 2000), measurement of crystal-field splitting (Garvie and Craven 1994), and bonding information (Brydson et al. 1998; van Aken et al. 1999a; Garvie and Buseck 1999a; Docherty et al. 2001). Information on the bonding is inherent in the shapes of the core-loss edges called the energy-loss near-edge structure (ELNES). The ELNES reflects the unoccupied, site-, and angular-momentum-projected DOS. Some recent examples demonstrate the utility of EELS for providing bonding information in materials (see Keast et al. 2001 for a detailed review). While a core-loss edge provides important information about a single atom, a unified picture of the unoccupied states is obtained by alignment of several core-loss spectra from the same material on a common energy scale. This alignment allows similarities between the ELNES of different atoms to be related to mixing of local conduction-band states.

Here we present and compare the EELS spectra of a transition metal (TM) sulfide. Pyrite was chosen because the basic features of the electron states are well known and thus suited for interpretation of the core-loss edges. Our goals are to record all core-loss EELS spectra of pyrite and illustrate differences in spectral shapes for the different core-loss edges. We discuss the theories necessary to understand the various core-loss edge shapes and in the process provide a clear picture of the conduction-band states as a function of energy above the band gap. This analysis reveals the extent of mixing of unoccupied state orbitals and thus provides an understanding of the limits of interpreting core-loss edges in light of the $\Delta l \pm 1$ limit. An essential component to understanding the EELS data is a comparison with the results of other spectroscopies that map the unoccupied states and with the results of band-structure calculations.

Experimental methods

A piece of a large cube of pyrite was crushed in methanol and a small drop of the fine mineral suspension was dried on a lacey C film. The pyrite was checked by powder X-ray diffraction and EDX in the TEM. Only Fe and S were detected by EDX and EELS.

Spectra were acquired with a GATAN 766DigiPEELS spectrometer attached to a Philips 400-ST field emission gun (FEG) TEM operated at an accelerating voltage of 100 kV. The width at half maximum, and hence the energy resolution, of the zero-loss peak depends on the current drawn from the FEG. Spectra up to an energy loss of 1000 eV were acquired with an energy resolution of ca. 0.8 eV, with current densities of ca. 5 nA. Current densities >10 nA were needed to record the S and Fe *K* signals, and so the FEG tip was operated with thermal assistance and high extraction voltage resulting in an energy resolution of ca. 1.5 eV. Spectra were acquired in diffraction mode (the spectrometer is image coupled), thus allowing control of the collection angle, 2α. In this mode, the objective point for the spectrometer is a specimen image at the strongly excited projector lens.

Typically, seven spectra were acquired for each edge, but with each spectrum shifted in energy relative to the previous one, in order to suppress the channel-to-channel gain variations. A dark-current spectrum was subtracted from each core-loss spectrum, and these spectra were then aligned and summed. A background of the form AE^{-r} was subtracted from beneath the S $L_{2,3}$ and *K* and Fe *K*, $M_{2,3}$, and $L_{2,3}$ edges. Use of the standard AE^{-r} power-law background subtraction technique was not suitable for the S L_1 and Fe M_1 edges because they are of weak intensity and sit on the intense tails of the preceding S $L_{2,3}$ and Fe $M_{2,3}$ edges, respectively. In order to remove the background we used the modified power-law background subtraction routines described by Egerton and Malac (2002). Following background subtraction the effects of the tailing of the zero-loss peak were deconvoluted using a point-spread-function spectrum. Further details of the spectrum acquisition and processing is given in Garvie and Buseck (1999a).

Spectrum acquisition parameters depended on the energy of the core-loss edge. Core-loss edges up to and including the Fe $L_{2,3}$ edge were acquired with a 0.2 eV dispersion, integration times of 1 to 3 s, collection half-angle of 10 mrad, and < 5nA probe current. Since the intensity of the energy-differential cross section varies approximately as E^{-2} (Egerton 1996), where *E* is the energy of the core-loss edge, longer acquisition times were acquired for the higher energy-loss features. The S *K* edge was acquired with 0.5 eV dispersion, 16 mrad collection half angle, 20 s integration time, and 10 nA probe current. The weak Fe *K* edge was acquired with 1 eV dispersion, 25 mrad collection half angle, 120 s integration time, and 20 nA probe current.

Pyrite is exceptionally beam-stable. No damage effects were observed, even for the long acquisition times necessary to record the S and Fe *K* edges. No orientation effects were observed in the ELNES.

Results

The core-loss edges exhibit a range of shapes (Figs. 1, 2, and 3) over a 7000 eV energy-loss region.

The Fe $M_{2,3}$ edge (Fig. 1a) sits on the tail of the plasmon peak,

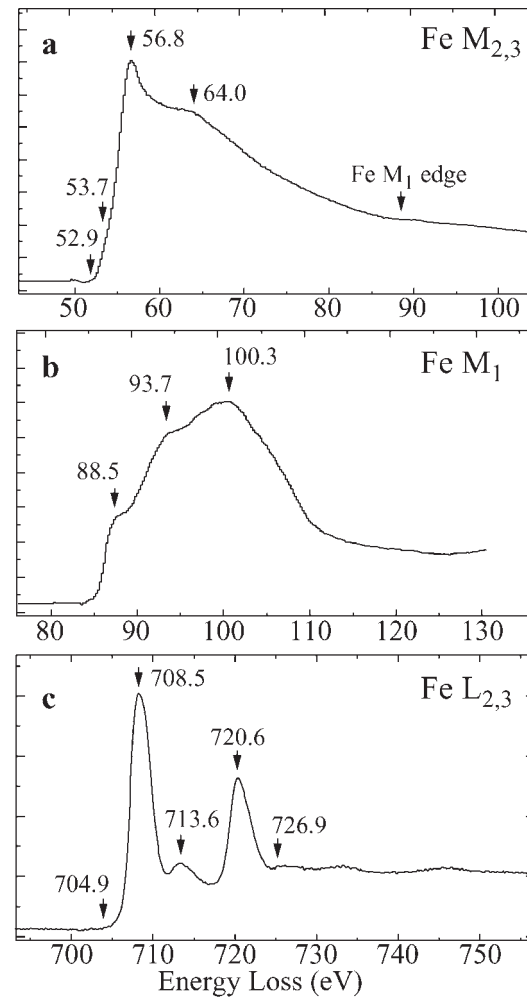

Figure 1. Iron core-loss edges of pyrite. The energies of the primary features are indicated on each spectrum.

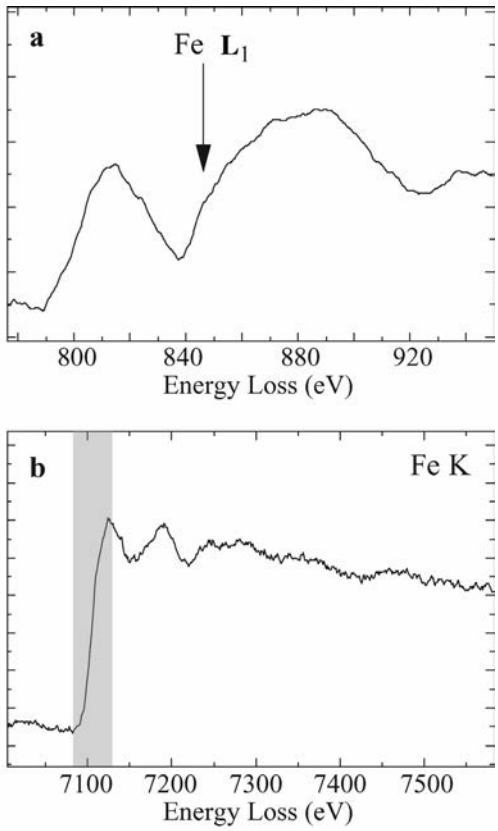

FIGURE 2. The Fe L_1 edge (**a**) and K edge (**b**) of pyrite. The L_1 edge is visible as a change in slope on the Fe $L_{2,3}$ EXELFS. The background beneath the EXELFS was subtracted using the cfit routine of Egerton and Malac (2002). The Fe K edge exhibits broad, intense EXELFS oscillations. The shaded region shows the location of the near-edge region.

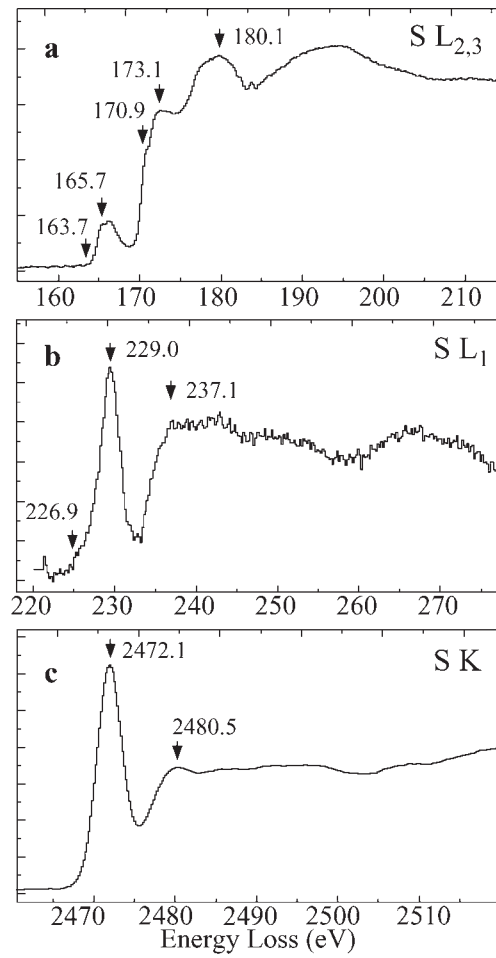

FIGURE 3. Sulfur core-loss edges of pyrite acquired by EELS. The energies of the primary features are indicated on each spectrum.

with an abrupt rise in intensity, one sharp maximum, followed by several weak oscillations. Just above the $M_{2,3}$ edge onset is a change in slope corresponding to a weak partially resolved maximum.

Weak intensity starting near 90 eV corresponds to a combination of the M_1 edge (Fig. 1b) and the beginning of the Fe $M_{2,3}$ extended energy-loss fine structure (EXELFS). No other elements that are likely in pyrite have core-loss edges with an onset near 90 eV. EDX spectra of the crystal studied did not reveal any elements other than Fe and S. The features arising from the M_1 edge can be separated from the EXELFS features because of the narrow width of the peaks centered at 88.5 and 93.7 eV, with ca. 2 to 3 eV full width at half maximum. The narrowness of these features excludes an EXELFS origin. The intensities of the M_1 edge maxima show a strong dependence on the method of background subtraction beneath the edge, although the absolute energies of the maxima remain constant.

The Fe $L_{2,3}$ edge (Fig. 1c) has a characteristic two-peaked structure with maxima for both the L_3 and L_2 edges. Following the main L_3 and L_2 are weaker satellite peaks. This edge has a similar shape to that recorded by X-ray absorption spectroscopy (XAS) (Mosselmans et al. 1995; Charnock et al. 1996; Womes et al. 1997; Todd et al. 2003).

The weak Fe L_1 edge at ca. 844 eV cannot be separated from the intense Fe $L_{2,3}$ EXELFS (Fig. 2a). It is visible on the Fe $L_{2,3}$ EXELFS as a change in slope at 845 eV.

The Fe K edge exhibits the characteristic saw-tooth shape, with an abrupt rise and then gradual decrease in spectral intensity (Fig. 2b). The energy region above ca. 2000 eV is usually the regime of XAS, because of the low spectral intensity of the high-energy loss spectra. Previous studies have shown that the 3*d TM* K edges are accessible by EELS (Hug et al. 1995).

Weak but sharp peaks that are separated by 0.9 eV follow the S $L_{2,3}$ edge onset (Fig. 3a). The bulk of the S $L_{2,3}$ edge intensity occurs above the trough at 169 eV. There are a series of peak maxima that comprise the ELNES up to 195 eV, which is followed by the EXELFS region. The S $L_{2,3}$ edge acquired by XAS and EELS are similar in shape (Li et al. 1995; Todd et al. 2003).

The S K edge is well resolved, with a white-line-like peak (Fig. 3c). Following this peak the intensity drops to a minimum before rising again to produce a series of weaker oscillations. A similar spectrum is recorded by XAS (Mosselmans et al. 1995; Womes et al. 1997; Bonnin-Mosbah 2002). The S L_1 edge has a white-line-like feature followed by broader less-intense maxima

(Fig. 3b). The S L_1 and K spectra are similar in shape and the white-line like feature at both edges have the same shape and peak width. Differences in spectral intensity between the S L_1 and K spectra following the white line are likely caused by the difficulty of removing the S $L_{2,3}$ EXELFS from beneath the L_1 edge.

Discussion

Origin of the core-loss edges

The basic core-loss edge shapes are dictated by atomic physics and are independent of the environment of the bonding or the atom. For isolated atoms, calculations show that K edges have a characteristic saw-tooth shape, $L_{2,3}$ edges of elements Na to Cl have a more rounded profile, and fourth-period elements have distinctive $L_{2,3}$ edges that are sharply peaked at the ionization threshold (Egerton 1996). In a solid these edge shapes are modified and exhibit a series of pronounced peaks within ca. 50 eV of the edge onset that are caused by the effects of the local electronic environment.

For core-loss edges of many elements, interpretation can be based on the one-electron approximation in which it is assumed that the excitation process has no effect on the remaining electrons in the atom and that all electrons experience the same effective potential. The edges can then be interpreted by comparing the ELNES with the density of states derived from a band-structure calculation (e.g., Womes et al. 1997). However, the single-electron model fails to adequately describe many core-loss edge features because of the modification of the unoccupied density of states by the effects of the excitation process and subsequent relaxation process (Brydson 1991).

The creation of the core-hole and subsequent relaxation processes are called many-body effects and include, for instance, the response of the passive electrons to the production of a core hole in the inner shell, interactions between the core hole and the ejected electron, and interactions between electrons in the final state. The magnitude of many-body effects vary and can be important, as in the 3*d TM* $L_{2,3}$ edges, or negligible as in many metallic systems. For elements of low atomic number, the core hole can have considerable influence on the spectral shape (Duscher et al. 2001).

In the following discussion, each core-loss edge of pyrite is discussed in terms of the basic physics that produces the main edge shape, many-body effects, and orbital character of the near-edge features.

***K*, L_1, and M_1 edges.** The characteristic saw-tooth shape of the S and Fe K edges is evident when viewed over an extended energy-loss range (Fig. 2b). This saw-tooth shape is not visible for the S L_1 edge because of the difficulty of subtracting the background from beneath the edge, as discussed above. The shape of the K edge is modified by the local electronic environment, which produces near-edge fine structure. The $\Delta l \pm 1$ dipole-rule states that the primary features of the K and L_1 ELNES arise from transitions of 1s electrons to unoccupied states of p-like character.

Both the S K and L_1 edges exhibit a sharp narrow peak at edge onset caused predominantly by transitions to antibonding p states. The dip in the spectral intensity following the peak maxima reflects the decrease in the number of states with p character with increase in energy above E_F. The origin of the maximum at 2480.5 eV corresponds to higher energy unoccupied p states, mixed with unoccupied Fe s states (Womes et al. 1997). A series of relatively weak, broad oscillations occur above 2486 eV, which form by scattering of the ejected electron from nearest-neighbor atoms and gives rise to the EXELFS oscillations.

The bulk of the Fe K ELNES can be attributed to dipole-allowed $s \rightarrow p$ transitions, mixed with some S d states because of the strong metal d-anion p mixing (Mosselmans et al. 1995; Womes et al. 1997). The pre-peak has weak intensity compared to the bulk of the K edge and is attributed to quadrupole $1s \rightarrow 3d$ transitions (Westre et al. 1997).

The Fe M_1 edge (Fig. 1b) represents transition of Fe 3s electrons to unoccupied p-like states. Previous studies of the 3*d TM* M_1 edge did not find significant intensity at the M_1 threshold for low-momentum transfers, but weak sharp peaks were observed at larger momentum transfer, $\mathbf{q} > 1$ Å^{-1} (Grunes and Leapman 1980).

Sulfur $L_{2,3}$ edge. This edge has a typical rounded profile, with a maximum ca. 20 eV above the edge onset (Fig. 3a). The d electron has an extra potential to surmount due to its angular momentum creating what is called a centrifugal barrier. At energies just above the ionization threshold, this centrifugal barrier prevents overlap between the initial 2p and final-state wave functions until the energy of the ejected electron is high enough to surmount it (Egerton 1996).

The spectral regions of the S $L_{2,3}$ edge include the weak pre-peak, followed by a decrease in spectral intensity and then a sharp rise corresponding to the main edge. The main peak intensity is attributed to transitions that are dipole in nature, S $p \rightarrow d$ (Muscat et al. 2002), mixed with orbital character from the Fe p orbitals (Womes et al. 1997). At the edge onset is a pair of peaks with weak intensity compared to the main edge. The transitions for the pre-peak are attributed to dipole-allowed $p \rightarrow s$, with enhancement of the intensity by monopole $p \rightarrow p$ transitions. The monopole enhancement reflects the s-p hybrid S bond. The pre-peak is split by 0.9 eV, which is caused by spin-orbit splitting. The two peaks therefore arise from transitions from $2p_{3/2}$ and $2p_{1/2}$ levels.

Iron $L_{2,3}$ edge. This edge exhibits two main peaks (Fig. 1c) that arise from transitions from the $2p_{3/2}$ ($j = 3/2$, L_3 edge) and $2p_{1/2}$ ($j = 1/2$, L_2 edge) levels; the energy separation between L_3 and L_2 is equal to the spin-orbit splitting. These two peaks arise from the two ways that the spin quantum number, s, can couple with the orbital angular momentum quantum number, l, to give the total angular momentum $j = l + s$. Unlike the other core-loss edges, a simple unoccupied DOS explanation cannot be used to describe the Fe $L_{2,3}$ edge. Instead, the large electron correlation in atoms with partially filled 3d shells precludes the use of a one-particle DOS to describe the $L_{2,3}$ edges (Brydson 1991).

For dominantly ionic systems, the atomic multiplet approach successfully describes the 3d $L_{2,3}$ edges (de Groot et al. 1990). It takes into account the dipole transition from the $2p^6 3d^n$ initial state to the $2p^5 3d^{n+1}$ final state, the 2p-3d and 3d-3d Coulomb and exchange interactions, the 2p and 3d spin-orbit interactions, and the effects of the crystal field. The atomic multiplet method has been successfully used to model spectra of Fe bonded to O in materials in which the Fe-O bond is predominantly ionic (van

der Laan and Kirkman 1992; Charnock et al. 1996).

For more covalent materials, e.g., the Fe chalcogenides, the atomic multiplet approach is less suitable (Charnock et al. 1996), and a more complicated configuration-interaction calculation including the charge transfer effects in the ground state have to be performed. In a bond with substantial covalency, the "sharing" of electrons can be understood in terms of electron transfer from anion to cation, with a mixed ground state of the form $2p^6 3d^6$ and $2p^6 3d^7 L$, where L refers to a hole in the S $2p$ valence band. In the final state, the $2p3d^7$ configuration is also strongly mixed with a $2p3d^8 L$ configuration. Interactions of the mixed ground and final states produce the main L_3 and L_2 peaks followed by satellite peaks.

The Fe L_3 and L_2 satellite peaks reveal an Fe-S bond with a substantial degree of mixing between d^6 and d^7 states for Fe. Such peaks have also been observed at other edges, such as the Ce $M_{4,5}$ edge of CeO_2 (Kotani and Ogasawara 1997; Garvie and Buseck 1999b). Thus, the main L_3 peak results from $p \rightarrow d$ transitions, while its satellite peak derives from a combination of dipole $p \rightarrow d$ and monopole $p \rightarrow p$ transitions.

Iron $M_{2,3}$ edge. The $3d$ *TM* $M_{2,3}$ edge differs in shape to the corresponding $L_{2,3}$ edge (Fig. 1) because the discrete $3p$ energy level interferes with the broad continuum states, εd, producing a broad asymmetric edge called a Fano resonance (Fano 1961; Jach and Girvin 1983). Constructive interference between the bound and continuum states accounts for the large peak intensity at the Fe $M_{2,3}$ peak onset. Therefore, the spectrum cannot be simply described in terms of the empty DOS. Close to the peak onset a pronounced minimum occurs at an energy where the transition amplitudes of the discrete state and the continuum interfere destructively.

Although the $M_{2,3}$ ELNES cannot be compared with the results of a DOS calculated by a one-electron band-structure method, this edge does exhibit valence-specific structure because the continuum states are influenced by the oxidation state (van der Laan 1991; van Aken et al. 1999b). A calculation using a localized description for the $3d^n$ to $3p^3 3d^{n+1}$ excitation that includes $3p$ and $3d$ spin-orbit interaction in octahedral symmetry successfully reproduces the main Fe $M_{2,3}$ edge shape of pyrite (van der Laan 1991).

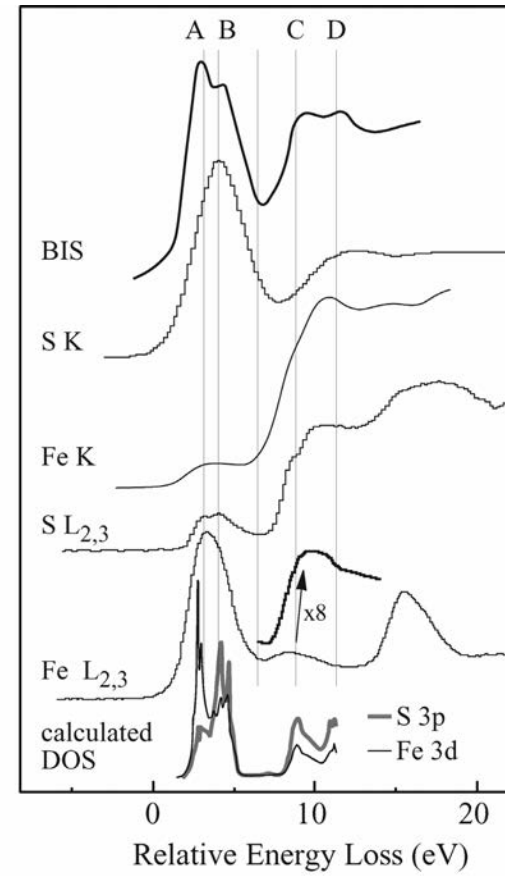

FIGURE 4. Alignment of the core-loss edges of pyrite and comparison with the BIS spectrum and the calculated unoccupied states. The Fe K edge acquired by XAS (Womes et al. 1997) is shown instead of that acquired by EELS because of the higher energy resolution of the XAS spectrum. The Fe $M_{2,3}$ edge is not shown because the significant interaction between the bound and continuum states produces the intense Fano resonance, which cannot be easily interpreted in terms of a simple DOS. In addition, the S L_1 edge is not shown because it has the same shape as the corresponding K edge. The hybridization satellite of the Fe L_3 edge is shown on an expanded scale for comparison with the other spectra. The letters A through D refer to features described in the text. Calculated unoccupied DOS adapted from Raybaud et al. (1997). Bremstrahlung isochromat spectrum (BIS) adapted from Folkerts et al. (1987).

ELNES interpretation

Band structure calculations of pyrite reveal a conduction band with strong contributions from Fe $3d$ and S $3p$ states between ca. 1 and 4 eV, a ca. 2 eV gap with low DOS, and an increase in states that are dominated by S states (Eyert et al. 1998; Muscat et al. 2002). The lowest part of the conduction band can be further separated into the 1.5 to 3 eV region with strong contributions from Fe $3d$ states, and the 3 to 4 eV region that is dominated by S $3p$ states (Eyert et al. 1998). Above ca. 7 eV the conduction band has significant contributions from S $3d$ states. These calculations reveal strong hybridization between the S $3p$ band and the nearly dispersion-less e_g band.

This division of the lower 5 eV of the conduction band into two parts is clearly visible from the Bremsstrahlung isochromat spectrum (BIS) (Fig. 4), and also with the ultraviolet inverse photoemission spectrum (Puppin et al. 1992). A BIS spectrum maps the total unoccupied DOS as a function of energy without influence of a core-hole potential (Fuggle 1992). The pyrite BIS spectrum (Folkerts et al. 1987) exhibits a broad peak with four maxima, peaks A, B, C and D. Peak A derives from transitions to Fe e_g states, with some S $3p_z$ and $3p_x + 3p_y$ contribution, and peak B from S $3p_z$ mixed with Fe $3d$ e_g and minor t_{2g}. The S $3s$ states make little contribution to the lower part of the conduction band (Eyert et al. 1998). The separation of the Fe d- and S p-derived peaks of the BIS spectrum is predicted by the calculated separation between the Fe $3d$ e_g and S $3p$ bands (Opahle et al. 1999, 2000).

Alignment of the core-loss edges of pyrite on a common energy scale (Fig. 4) allows similarities between the ELNES of the different atoms to be related to mixing of conduction-band states. Similar alignments were done for the Fe K, L_3, and S K (Mosselmans et al. 1995; Womes et al. 1997) and S K, $L_{2,3}$, and

Fe *K* (Li et al. 1995) edges acquired by XAS from pyrite. Peaks at similar energies represent transitions to mixed states or at least states of similar energy. Since the primary orbital character of the first feature in each core-loss edge is known, they are aligned with the corresponding feature in the BIS spectrum and DOS plot. The white-line peak maximum of the S *K* edge, which is assigned to unoccupied 3*p* states (Womes et al. 1997), is aligned with peak B of the BIS spectrum. Similarly, the main Fe L_3 peak maximum represents transitions to unoccupied *d*-states is aligned with peak A of the BIS spectrum. The maxima of the Fe L_3 and S *K* edges are separated by ca. 1 eV reflecting the separation between peaks A and B in the BIS spectrum and partial DOS plot. Since the small pre-peak to the Fe *K* edge arises primarily from $1s \rightarrow d$ transitions it is aligned with peak A of the BIS spectrum. The first peak of the S $L_{2,3}$ edge is dominated by transitions from S $2p \rightarrow 3p$ states, and so the first maximum is aligned with peak B of the BIS spectrum.

In the aligned spectra, the origin of the energy scale is taken at the bottom of the Fermi level, E_F. The aligned EELS spectra clearly divide the unoccupied states into two regions below and above 5 eV, which is also matched by the energy separation in the BIS (Folkerts et al. 1987) spectrum and DOS plot (Raybaud et al. 1997). A minimum in EELS spectral intensity separates these two energy regions. In doing this alignment, we find remarkable concurrence among the spectral features above the 5-eV minimum and to the BIS spectrum and DOS plot (Fig. 4). Comparing the Fe *K* and S $L_{2,3}$ edges above C, we observe similar edge shapes up to ca. 12 eV and conclude that Fe *p* states are hybridized with S *d* orbitals. There is also close correspondence between the S and Fe *K* edge spectral features from 5 to 12 eV. It is therefore concluded that the S *K* edge structures in this region represents hybridized S and Fe *p* states.

The Fe L_3 hybridization satellite has a rise in intensity, and a broad maximum that parallels that seen at the Fe *K* and S $L_{2,3}$ edges above 5 eV. This similarity confirms its origin as arising from Fe–S covalency. This interpretation is in contrast to that given by Womes et al. (1997), who attribute this structure to transitions of Fe $2p \rightarrow 4s$. The high degree of covalency of the Fe–S bond results in an hybrid Fe $L_{2,3}$ edge that has the overall features of an $L_{2,3}$ edge arising from quasiatomic transitions, but with significant modification caused by the high degree of the Fe $3d\ e_g$ – S 3*p* overlap. Thus, this overlap results in the formation of ELNES features that align with structures belonging to the other edges with which the Fe 3*d* electrons mix.

The correlations between different EELS spectra of the same material is shown to be effective at probing the nature of empty conduction band states just above the Fermi level. Analysis of the ELNES is a powerful method of understanding the distribution of states and the degree of mixing of these states. Similar data are obtained by comparison of XAS spectra since both XAS and EELS probe the atom-resolved, partial density of unoccupied states. One advantage of superimposing the various spectra is the identification of higher-energy unoccupied states. These states are not normally accessible by ab initio calculations, which usually only include the first ca. 5 eV above the Fermi level.

Alignment of the edges on a common energy scale reveals a conduction band that is split into two regions. A lower-energy region between 0 and 5 eV in which there are distinct and separated ELNES features corresponding to transitions to S *p* (*K* edge) and Fe *d* (L_3 edge) states. Weaker features in this region at the Fe *K* and S $L_{2,3}$ edges attest to mixing of Fe *p*, *d*, and S *s* and *p* states. And the higher energy conduction band states above 5 eV, in which there is close correspondence of all spectral features of the edges implying substantial mixing of Fe and S states.

ACKNOWLEDGMENTS

We are grateful to P. Rez for his many helpful discussions and to the reviewers P.A. van Aken and A. Baronnet for their careful reviews. Funding was provided by the National Science Foundation NSF EAR 00-87714 and 01-13345.

REFERENCES CITED

Bonnin-Mosbah, M., Métrich, N., Susini, J., Salomé, M., Massare, D., and Menez, B. (2002) Micro X-ray absorption near edge structure at the sulfur and iron K-edges in natural silicate glasses. Spectrochimica Acta B, 57, 711–725.

Brydson, R. (1991) Interpretation of near-edge structure in the electron energy-loss spectrum. EMSA Bulletin, 21, 57–67.

Brydson, R., Brown, L.M., and Bruley, J. (1998) Characterizing the local nitrogen environment at platelets in type IaA/B diamond. Journal of Microscopy–Oxford, 189, 137–144.

Charnock, J.M., Henderson, C.M.B., Mosselmans, J.F.W., and Pattrick, R.A.D. (1996) 3d transition metal L-edge x-ray absorption studies of the dichalcogenides of Fe, Co and Ni. Physics and Chemistry of Minerals, 23, 403–408.

Collison, D., Garner, C.D., McGrath, C.M., Mosselmans, J.F.W., Roper, M.D., Seddon, J.M.W., Sinn, E., and Young, N.A. (1997) Soft x-ray induced excited spin state trapping and soft X-ray photochemistry at the iron $L_{2,3}$ edge in $[Fe(phen)_2(NCS)_2]$ and $[Fe(phen)_2(NCSe)_2]$ (phen = 1,10-phenanthroline). Journal of Chemistry, Dalton Transactions, 4371–4376.

Docherty, F.T., Craven, A.J., McComb, D.W., and Skakle, J. (2001) ELNES investigations of the oxygen K-edge in spinels. Ultramicroscopy, 86, 273–288.

Duscher, G., Buczko, R., Pennycook, S.J., and Pantelides, S.T. (2001) Core-hole effects on energy-loss near-edge structure. Ultramicroscopy, 86, 355–362.

Egerton, R.F. (1996) Electron Energy-Loss Spectroscopy in the Electron Microscope (Second Edition). Plenum Press, New York.

Egerton, R.F. and Malac, M. (2002) Improved background-fitting algorithms for ionization edges in electron energy loss spectra. Ultramicroscopy, 92, 47–56.

Ennaoui, A., Fiechter, S., Pettenkofer, C., Alonsovante, N., Buker, K., Bronold, M., Hopfner, C., and Tributsch, H. (1993) Iron disulfide for solar-energy conversion. Solar Energy Materials and Solar Cells, 29, 289–370.

Eyert, V., Höck, K.H., Fiechter, S., and Tributsch, H. (1998) Electronic structure of FeS_2: the crucial role of electron-lattice interaction. Physical Review B, 57, 6350–6359.

Fano, U. (1961) Effects of configuration interaction on intensities and phase shifts. Physical Review, 124, 1866–1878.

Ferrer, I.J., Nevskaia, D.M., de las Heras, C., and Sanchez, C. (1990) About the band gap nature of FeS_2 as determined from optical and photoelectrochemical measurements. Solid State Communications, 74, 913–916.

Folkerts, W., Sawatzky, G.A., Haas, C., de Groot, R.A., and Hillebrecht, F.U. (1987) Electronic structure of some 3D transition-metal pyrites. Journal of Physics C: Solid State Physics, 20, 4135–4144.

Frost, D.J., Langenhorst, F., and van Aken, P.A. (2001) Fe-Mg partitioning between ringwoodite and magnesiowustite and the effect of pressure, temperature and oxygen fugacity. Physics and Chemistry of Minerals, 28, 455–470.

Fuggle, J.C. (1992) Bremsstrahlung isochromat spectroscopy (BIS or high-energy inverse photoemisson). Topics in Applied Physics, 69, 307–337.

Garvie, L.A.J. and Buseck, P.R. (1998) Ferrous/ferric ratios from nanometer-sized areas in minerals. Nature, 396, 667–670.

——— (1999a) Bonding in silicates: Investigation of the Si $L_{2,3}$-edge by parallel electron energy-loss spectroscopy (EELS). American Mineralogist, 84, 946–964.

——— (1999b) Electron-beam induced solid-state reduction of Ce(IV) to Ce(III) in cerianite (CeO_2) studied by electron energy-loss spectroscopy (EELS). Journal of Physics and Chemistry of Minerals, 60, 1943–1947.

Garvie, L.A.J. and Craven, A.J. (1994) High resolution parallel electron energy-loss spectroscopic study of Mn $L_{2,3}$ edges in inorganic manganese compounds. Journal of Physics and Chemistry of Minerals, 21, 191–206.

Garvie, L.A.J., Craven, A.J., and Brydson, R. (1994) Use of electron-loss near-edge fine structure in the study of minerals. American Mineralogist, 79, 411–425.

Gloter, A., Guyot, F., Martinez, I., and Colliex, C. (2000) Electron energy-loss spectroscopy of silicate perovskite-magnesiowustite high-pressure assemblages. American Mineralogist, 85, 1452–1458.

de Groot, F.M.F., Fuggle, J.C., Thole, B.T., and Sawatzky, G.A. (1990) 2p X-ray absorption of 3d transition-metal compounds: an atomic multiplet description including the crystal field. Physical Review B, 42, 5459–5468.

Grunes, L.A. and Leapman, R.D. (1980) Optically forbidden excitations of the 3s

subshell in the 3d transition metals by inelastic scattering of fast electrons. Physical Review B, 22, 3778–3783.
Hansen, P.L., Brydson, R., McComb, D.W., and Richardson, I. (1994) EELS fingerprint of Al-coordination in silicates. Microscopy Microanalysis Microstructures, 5, 173–182.
de las Heras, C. and Lifante, G. (1997) Optical parameters of pyrite thin films. Journal of Applied Physics, 82, 5132–5137.
Hug, G., Blanche, G., Jaouen, M., Flank, A.M., and Rehr, J.J. (1995) Simulation of the extended fine structure of the K-shell edges in intermetallic ordered alloys. Ultramicroscopy, 59, 121–136.
Jach, T. and Girvin, S.M. (1983) Momentum-transfer dependence of Fano line shape in electron-energy-loss spectra of nickel. Physical Review B, 27, 1489–1492.
Keast, V.J., Scott, A.J., Brydson, R., Williams, D.B., and Bruley, J. (2001) Electron energy-loss near-edge structure—a tool for the investigation of electronic structure on the nanometer scale. Journal of Microscopy – Oxford, 203, 135–175.
Kotani, A. and Ogasawara, H. (1997) Interplay between intra-atomic multiplet coupling and interatomic hybridization in core-level spectroscopy. Journal of Electron Spectroscopy and Related Phenomena, 86, 65–72.
Li, D., Bancroft, G.M., Kasrai, M., Fleet, M.E., Feng, X., and Tan, K. (1995) S K- and L-edge X-ray absorption spectroscopy of metal sulfides and sulfates: applications in mineralogy and geochemistry. Canadian Mineralogist, 33, 949–960.
Mosselmans, J.F.W., Pattrick, R.A.D., van der Laan, G., Charnock, J.M., Vaughan, D.J., Henderson, C.M.B., and Garner, C.D. (1995) X-ray absorption near-edge spectra of transition metal disulfides FeS_2 (pyrite and marcasite), CoS_2, NiS_2 and CuS_2, and their isomorphs FeAsS and CoAsS. Physics and Chemistry of Minerals, 22, 311–317.
Muscat, J., Hung, A., Russo, S., and Yarovsky, I. (2002) First-principle studies of the structural and electronic properties of pyrite FeS_2. Physical Review B, 65, no. 054107.
Opahle, I., Koepernik, K., and Eschrig, H. (1999) Full-potential band-structure calculation of iron pyrite. Physical Review B, 60, 14035–14041.
——— (2000) Full potential band structure calculation of iron pyrite. Computational Materials Science, 17, 206–210.
Puppin, E., Finazzi, M., and Ciccacci, F. (1992) Ultraviolet inverse photoemission from FeS_2. Solid State Communications, 82, 489–491.
Raybaud, P., Hafner, J., Kresse, G., and Toulhoat, H. (1997) Ab initio density functional studies of transition-metal sulphides: II. Electronic structure. Journal of Physics: Condensed Matter, 9, 11107–11140.
Sato, K. (1984) Reflectivity spectra and optical constants of pyrites (FeS_2, CoS_2, and NiS_2) between 0.2 and 4.4 eV. Journal of the Physical Society of Japan, 53, 1617–1620.
Schmidbeurmann, P. and Lottermoser, W. (1993) Fe-57 Mossbauer spectra, electronic and crystal-structure of members of the CuS_2-FeS_2 solid-solution series. Physics and Chemistry of Minerals, 19, 571–577.
Thole, B.T. and van der Laan, G. (1988) Linear relation between X-ray absorption branching ratio and valence-band spin-orbit expectation value. Physical Review A, 38, 1943–1947.
Todd, E.C., Sherman, D.M., and Purton, J.A. (2003) Surface oxidation of pyrite under ambient atmospheric and aqueous (pH = 2 to 10) conditions: electronic structure and mineralogy from x-ray absorption spectroscopy. Geochimica et Cosmochimica Acta, 67, 881–893.
van Aken, P.A. and Liebscher, B. (2002) Quantification of ferrous/ferric ratios in minerals: new evaluation schemes of Fe $L_{2,3}$ electron energy-loss near-edge spectra. Physics and Chemistry of Minerals, 29, 188–200.
van Aken, P.A., Wu, Z.Y., Langenhorst, F., and Seifert, F. (1999a) ELNES spectroscopy and XANES calculations of the O K edge: orientation dependence and effects of protons in $Mg(OH)_2$. Physical Review B, 60, 3815–3820.
van Aken, P.A., Styrsa, V.J., Liebscher, B., Woodland, A.B., and Redhammer, G.J. (1999b) Microanalysis of $Fe^{3+}/\Sigma Fe$ in oxide and silicate minerals by investigation of electron energy-loss near-edge structures (ELNES) at the Fe M_2,M_3 edge. Physics and Chemistry of Minerals, 26, 584–590.
van der Laan, G. (1991) $M_{2,3}$ absorption spectroscopy of 3d transition-metal compounds. Journal of Physics: Condensed Matter, 3, 7443–7454.
van der Laan, G. and Kirkman, I.W. (1992) The 2p absorption spectra of 3d transition metal compounds in tetrahedral and octahedral symmetry. Journal of Physics: Condensed Matter, 4, 4189–4204.
Westre, T.E., Kennepohl, P., DeWitt, J.G., Hedman, B., Hodgson, K.O., and Solomon, E.I. (1997) A multiplet analysis of Fe K-edge 1s → 3d pre-edge features of iron complexes. Journal of the American Chemical Society, 119, 6297–6314.
Womes, M., Karnatak, R.C., Esteva J.M., Lefebvre, I., Allan, G., Olivier-Fourcades, J., and Jumas J.C. (1997) Electronic structures of FeS and FeS_2: X-ray absorption spectroscopy and band structure calculations. Journal of Physics and Chemistry of Solids, 58, 345–352.
Zega, T.J., Garvie, L.A.J., and Buseck, P.R. (2003) Nanometer-scale measurements of iron oxidation states of cronstedtite from primitive meteorites. American Mineralogist, 88, 1169–1172.

MANUSCRIPT RECEIVED JULY 19, 2002
MANUSCRIPT ACCEPTED SEPTEMBER 25, 2003
MANUSCRIPT HANDLED BY ALAIN BARONNET